

# Photochemical & Photobiological Sciences

Accepted Manuscript



This is an *Accepted Manuscript*, which has been through the Royal Society of Chemistry peer review process and has been accepted for publication.

*Accepted Manuscripts* are published online shortly after acceptance, before technical editing, formatting and proof reading. Using this free service, authors can make their results available to the community, in citable form, before we publish the edited article. We will replace this *Accepted Manuscript* with the edited and formatted *Advance Article* as soon as it is available.

You can find more information about *Accepted Manuscripts* in the [Information for Authors](#).

Please note that technical editing may introduce minor changes to the text and/or graphics, which may alter content. The journal's standard [Terms & Conditions](#) and the [Ethical guidelines](#) still apply. In no event shall the Royal Society of Chemistry be held responsible for any errors or omissions in this *Accepted Manuscript* or any consequences arising from the use of any information it contains.

## Stepwise photoconversion of an artificial light-harvesting array built from extended BODIPY units

Cite this: DOI: 10.1039/x0xx00000x

Received 00th January 2012,  
Accepted 00th January 2012

DOI: 10.1039/x0xx00000x

[www.rsc.org/](http://www.rsc.org/)

Anthony Harriman,<sup>\*a</sup> Patrycja Stachelek,<sup>a</sup> Alexandra Sutter<sup>b</sup> and Raymond Ziessel<sup>\*b</sup>

A molecular dyad, comprising two disparate extended boron dipyrromethene (BODIPY) units, has been identified as a potential component of artificial light-harvesting arrays. Highly efficient, intramolecular electronic energy transfer takes place under illumination but there is some competition from light-induced electron transfer along the molecular axis. The primary energy acceptor has a somewhat shortened excited-state lifetime and reduced emission quantum yield due to charge transfer from a terminal amine residue, the latter being required for the molecular system to operate in organic solar cells. Under continuous illumination with simulated solar light, the dyad undergoes very slow decomposition. In a protic solvent, both BODIPY units degrade at the same rate via an autocatalytic process. The products, one of which is a protonated analogue of the donor, degrade further by independent routes. In aprotic solvents or thin plastic films, the acceptor BODIPY dye absorbing at lowest energy undergoes photochemical degradation as above but the donor is much more stable under these conditions. At each stage of degradation, the molecule retains the ability to sensitize an amorphous silicon solar cell and the overall turnover number with respect to absorbed photons exceeds 10 million. The optical properties of the target compound nicely complement those of the solar cell and sensitization helps to avoid Staebler-Wronski photo-degradation.

### Introduction

The process of electronic energy transfer (EET) has been used as the underlying methodology by which to engineer numerous analytical protocols,<sup>1</sup> chemical sensors,<sup>2</sup> bio-probes<sup>3</sup> and molecular machines.<sup>4</sup> Artificial light-harvesting devices,<sup>5</sup> as used to drive solar cells<sup>6</sup> and/or photochemical batteries,<sup>7</sup> also rely heavily on EET to channel photons to the desired location. For these latter systems to be viable, it is necessary that the highly efficient EET process is matched by exceptional stability under prolonged exposure to sunlight. Unfortunately, most organic materials that absorb and emit in the near-IR region, this being the most interesting window for the sensitization of solar cells,<sup>8</sup> degrade rather quickly under sustained illumination. We have, of late, become interested in seeking ways to stabilize certain classes of highly emissive dyes, most notably the boron dipyrromethene<sup>9</sup> (BODIPY) family that figures prominently in artificial light-harvesting arrays.<sup>5</sup> Here,

we provide a preliminary account of the photochemistry of one such elaborate molecular entity that absorbs across the entire visible region but emits solely in the near-infra-red region. The goal of the work is to examine ways to improve the stability of the device under continuous illumination with artificial solar light.

To test the system, we have developed a simple experimental set-up whereby the target compound is dispersed in a plastic block and used to sensitize an amorphous silicon (a-Si:H) cell. It is noted that thin film a-Si:H solar cells appear as promising alternatives to similar cells constructed from highly crystalline silicon wafers for photovoltaic power generation. In part, this is because of their low cost and facile fabrication but a serious disadvantage relates to their low solar-to-electricity conversion efficiency from. Because of the disordered nature of amorphous silicon, such solar cells are subject to the Staebler-Wronski effect,<sup>10</sup> which concerns recombination of charge not extracted from the cell, which causes structural damage and

reduces efficiency during the first 100 hours or so of operation. This distortion arises, at least to a large degree, by illumination with blue light and therefore might be avoided by sensitization with a far-red emitting dye.

## Results and Discussion

### Characterization and background studies

The target molecular array,<sup>8</sup> **1**, which is unusually large (molar mass equals 1,721 g/mol; solvent accessible surface area equals 910 cm<sup>2</sup>/mol), comprises two BODIPY-based components interconnected via a tolane linker (Figure 1). Both chromophores are built from styryl-BODIPY dyes<sup>9</sup> but differ in terms of their respective conjugation lengths, and hence their optical properties. The smaller terminal, BDMA, has a styryl-BODIPY unit equipped with a single *N,N*-dimethylaniline residue that is known<sup>11</sup> to function as a pH probe. The reference compound, **D1** (Figure 2), for this component absorbs intensely at about 600 nm and fluoresces with a maximum at about 710 nm in CH<sub>2</sub>Cl<sub>2</sub>. The fluorescence quantum yield ( $\Phi_F$ ) for **D1** in CH<sub>2</sub>Cl<sub>2</sub> at room temperature is 0.38 while the corresponding excited-singlet state lifetime ( $\tau_S$ ) is 3.7 ns. It might be noted that the emission properties, including the radiative rate constant ( $k_{RAD} = 1 \times 10^8 \text{ s}^{-1}$  in CH<sub>2</sub>Cl<sub>2</sub>) are sensitive to the dielectric constant of the surrounding solvent, due to the inherent charge-transfer character of this molecule, and also to the presence of adventitious protons.<sup>11</sup>

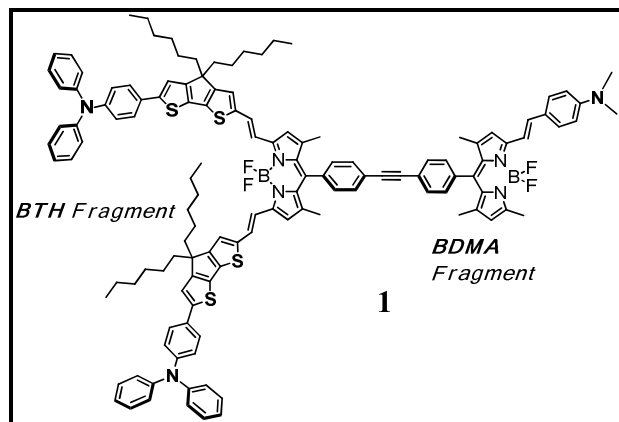
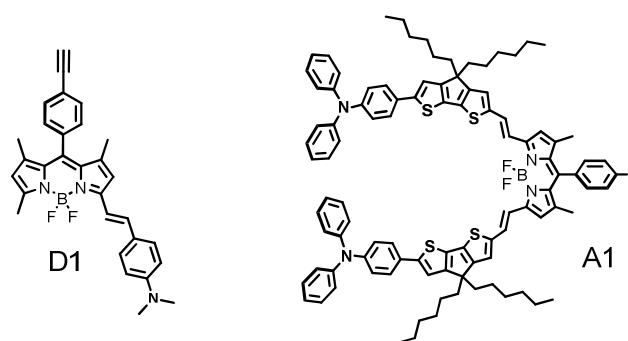


**Figure 1.** Molecular formula of the artificial light harvester, **1**, examined in this work. See Supporting Information for the energy-minimized geometry.

The complementary terminal is significantly larger with a more expansive conjugation pathway that pushes the lowest-energy absorption transition to about 815 nm. This unit, BTH, bears two fused thiophene fragments attached to the BODIPY dye via an ethene linkage. Fluorescence from this terminal is relatively weak, with  $\Phi_F = 0.013$  and  $\tau_S = 0.25 \text{ ns}$  in CH<sub>2</sub>Cl<sub>2</sub>, and has a maximum at 897 nm. The poor emission properties might reflect the low radiative rate constant ( $k_{RAD} = 5 \times 10^7 \text{ s}^{-1}$ ) associated with the near-IR spectral profile<sup>12</sup> but also there is the strong likelihood of intramolecular charge-transfer interactions between the appended groups. These latter units are

attached to the chromophore to enhance its performance in organic solar cells.<sup>13</sup> It should be noted that the photophysical properties recorded for the BTH unit present in **1** are closely comparable to those found for the isolated control compound **A1** (Figure 2), confirming that the restricted fluorescence is not a consequence of interaction with BDMA. The same conclusion cannot be reached for the corresponding BDMA terminal. Thus, fluorescence from **1** at around 700 nm is difficult to resolve from the baseline and corresponds to  $\Phi_F$  of  $<10^{-4}$ . The excited-state lifetime for this emission is reduced to  $<20 \text{ ps}$ . The two most obvious causes of this pronounced intramolecular fluorescence quenching are EET from BDMA to BTH and/or light-induced charge transfer along the molecular axis.

**Figure 2.** Molecular formulae for the isolated control compounds used to better understand the properties of the molecular array. See Supporting Information for the energy-minimized structures.



In consideration of intramolecular EET, it is noted that the relative positioning of excited-state energy levels, the close proximity of the chromophores, the centre-to-centre separation being 19.7 Å, and high spectral overlap integral<sup>14</sup> ( $J_{DA} = 0.0024 \text{ cm}$ ) calculated for **1** are somewhat offset by the modest orientation factor<sup>15</sup> ( $\kappa^2 = 0.15$ ). A conventional Förster-type calculation,<sup>16</sup> based on the ideal-dipole approximation, predicts a rate constant for intramolecular EET from BDMA to BTH of ca.  $1.5 \times 10^{11} \text{ s}^{-1}$ , while this value falls very slightly to  $1.4 \times 10^{11} \text{ s}^{-1}$  when the Kuhn extended dipole approach is used.<sup>17</sup> Furthermore, the excitation spectrum indicates that at least 80% of photons collected by the BDMA chromophore are transferred to the appended BTH unit. Thus, intramolecular EET from BDMA to BTH is likely to be highly efficacious.

In order to assess the significance of light-induced electron transfer within **1**, cyclic voltammograms were recorded in CH<sub>2</sub>Cl<sub>2</sub> containing background electrolyte. The main findings are summarized in Table 1 where the assignments are made on the basis of identical studies performed with the control compounds. Now, three peaks are observed on reductive scans. The first two reduction peaks are *quasi*-reversible and correspond to one-electron reduction of BTH and BDMA units, respectively, with half-wave potentials of -1.00 and -1.21 V vs SCE. The third reduction peak is irreversible and, by reference to the control compounds, corresponds to addition of a second electron to the BTH unit. A total of four oxidative processes

can be identified, each of which corresponds to the *quasi*-reversible removal of one electron from **1**. The first two peaks correspond to the generic oxidation of BTH and BDMA units, respectively, with half-wave potentials of 0.38 and 0.56 V vs SCE, as identified by comparison with the control compounds. The remaining two oxidation steps are difficult to assign simply by comparison with these same reference compounds and further information about the electronic nature of these chromophores was sought from molecular orbital calculations. It is also important to recognize that the acceptor comprises multiple discrete units that might not be in strong electronic communication. There is a need, therefore, to better understand how the redox equivalents introduced during the electrochemical processes are localized within the overall structure.

multiple discrete units that might not be in strong electronic communication. There is a need, therefore, to better understand how the redox equivalents introduced during the electrochemical processes are localized within the overall structure.

**Table 1.** Summary of the electrochemical properties recorded for **1** and the control compounds as recorded in CH<sub>2</sub>Cl<sub>2</sub> containing TBAP (0.1 M) as background electrolyte.

Cmpd	E <sup>0</sup> (ox, soln) (V), ΔE (mV) <sup>a</sup>	E <sup>0</sup> (red, soln) (V), ΔE (mV) <sup>b</sup>
D1	+0.54 (60), +0.87 (60)	-1.20 (60)
A1	+0.38 (60), +0.83 (60), +1.00 (60)	-1.00 (70), -1.63 (irr.) <sup>c</sup>
<b>1</b>	+0.38 (60), +0.56 (60), +0.84 (70), +1.00 (60)	-1.00 (80), -1.21 (70), -1.85 (irr.) <sup>c</sup>

(a) Refers to oxidative processes. (b) Refers to reductive processes.  
(c) N.B. irr means irreversible electrochemical step.

In order to assess the significance of light-induced electron transfer within **1**, cyclic voltammograms were recorded in CH<sub>2</sub>Cl<sub>2</sub> containing background electrolyte. The main findings are summarized in Table 1 where the assignments are made on the basis of identical studies performed with the control compounds. Now, three peaks are observed on reductive scans. The first two reduction peaks are *quasi*-reversible and correspond to one-electron reduction of BTH and BDMA units, respectively, with half-wave potentials of -1.00 and -1.21 V vs SCE. The third reduction peak is irreversible and, by reference to the control compounds, corresponds to addition of a second electron to the BTH unit. A total of four oxidative processes can be identified, each of which corresponds to the *quasi*-reversible removal of one electron from **1**. The first two peaks correspond to the generic oxidation of BTH and BDMA units, respectively, with half-wave potentials of 0.38 and 0.56 V vs SCE, as identified by comparison with the control compounds. The remaining two oxidation steps are difficult to assign simply by comparison with these same reference compounds and further information about the electronic nature of these chromophores was sought from molecular orbital calculations. It is also important to recognize that the acceptor comprises

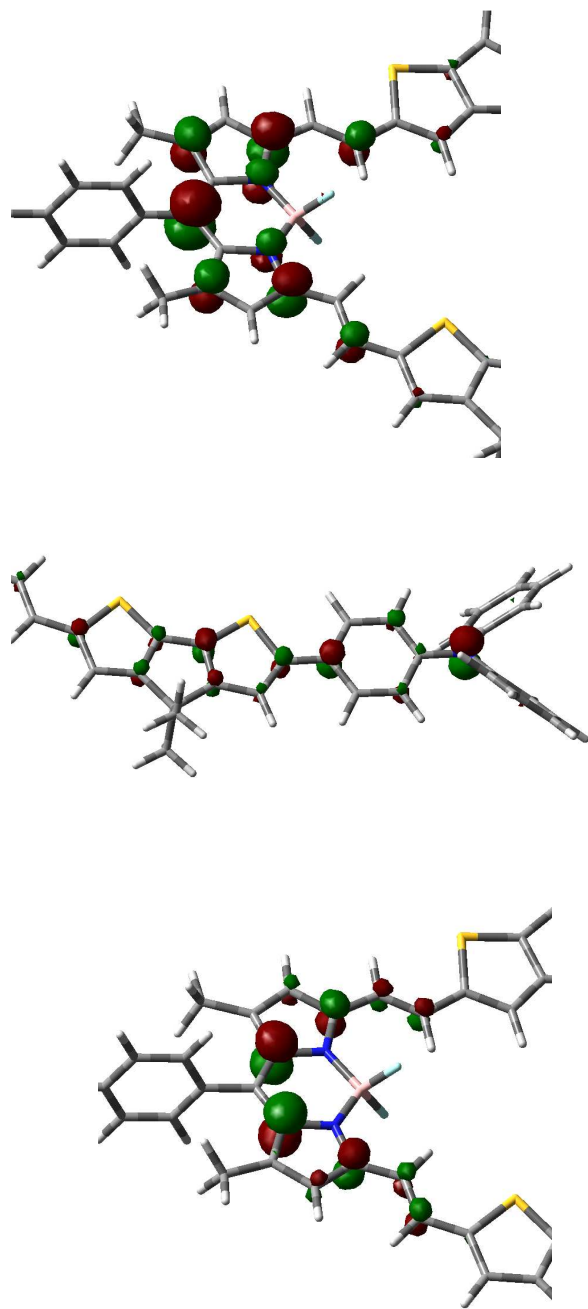


Figure 3. Kohn-Sham representations for **1** at isodensity of 0.015 for LUMO (upper), HOMO (centre) and HOMO(-2) (lower). NB The hexyl chains have been replaced with methyl groups.

Quantum chemical studies for BDMA have been described previously,<sup>11</sup> together with a few relevant compounds, and the main conclusion is that the entire molecule functions as an extended push-pull<sup>18</sup> electronic system. Charge transfer from

the N,N-dimethylanilino unit to the BODIPY nucleus serves to increase the molecular dipole moment ( $\mu$ ) at both ground (DFT/B3LYP/aug-cc-pVTZ:  $\mu = 3.0$  D) and excited-state (TD-DFT/CAM-B3LYP:  $\mu = 7.2$  D) levels while the wavenumber for the emission maximum decreases with increasing solvent polarity.<sup>11</sup> The control compound is highly sensitive to the presence of protons<sup>11</sup> and the resultant protonated species ( $\lambda_{\text{ABS}} = 553$  nm;  $\lambda_{\text{FLU}} = 561$  nm) is strongly fluorescent ( $\Phi_{\text{F}} = 1.0$ ). Related calculations were made for the acceptor component, **A1**, and indicate that the ground-state dipole moment is 1.6 D with little change on excitation. Interestingly, while the LUMO is essentially localized on the extended dipyrin nucleus, the HOMO is centred on the terminal amine (see Supporting Information). Moreover, HOMO(-1) is associated with the thiophene spacer and it is not until we reach HOMO(-2) that electron density is removed from the dipyrin unit (see Supporting Information). The same type of molecular orbital description is found for the full molecule **1** and partial MO pictures are shown below (Figure 3); see Supporting Information for the full molecule. This finding can be used to imply that the relatively short  $\tau_{\text{S}}$  and low  $\Phi_{\text{F}}$  found for the acceptor unit arise from intramolecular charge transfer with the appended amine.

Combining these orbital descriptions with the above-mentioned electrochemistry, it can be concluded that the only light-induced electron-transfer event able to compete with excited-state deactivation involves charge transfer from the excited-singlet state of BDMA to BTH. For this process, the thermodynamic driving force ( $\Delta G_{\text{CT}}$ ) is estimated<sup>19</sup> to be ca. 0.5 eV (see Supporting Information) and it is possible that this route contributes towards the missing 20% or so from the comparative excitation and absorption spectra. Our conclusion, therefore, is that intramolecular electron transfer might compete rather ineffectively with EET from BDMA to BTH for the target compound in a polar solvent. In nonpolar media, we might anticipate a severe reduction in the rate of charge transfer but no real effect on the efficacy of intramolecular EET.

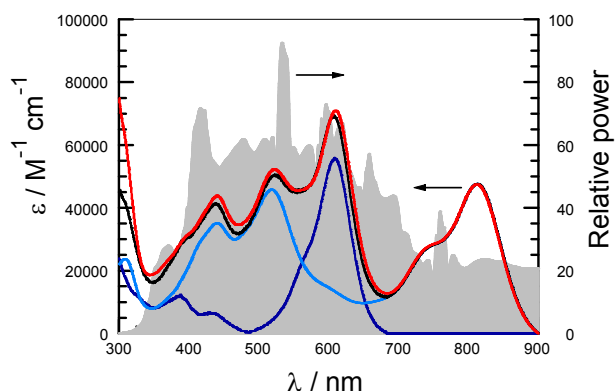


Figure 4. Absorption spectra recorded for **D1** (dark blue curve), **A1** (light blue curve), an equimolar mixture of **D1** and **A1** (black curve) and **1** (red curve) in  $\text{CH}_2\text{Cl}_2$  solution: the normalized lamp profile is shown as the shaded grey curve.

### Photochemical degradation

We now turn our attention to the main focus of this work, namely the effect of illumination with simulated sunlight on the target compound. Preliminary studies carried out with **1** dispersed in plastic films, such media being relevant for the sensitization of solar cells, indicated that the course of reaction was too slow to be followed in a meaningful manner. Photochemical bleaching in anaerobic organic solvents is slow but can be monitored by absorption spectroscopy. Of the available solvents,  $\text{CH}_2\text{Cl}_2$  is the most suitable in terms of solubility. Output from the lamp, filtered to remove  $\lambda < 340$  nm but otherwise covering the entire visible region (Figure 4), was directed to the front surface of the sample cell without focussing. It should be emphasized that both chromophores absorb incident light under these conditions. Integration of the individual spectral profiles and comparison with output from the lamp allows us to conclude that 32% of incident photons are collected by BDMA, with the remaining 68% being harvested by BTH.

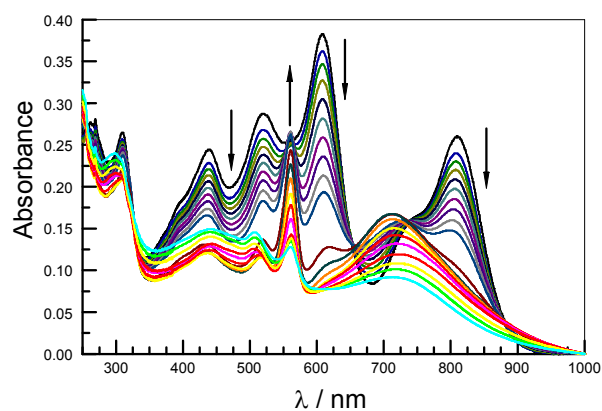


Figure 5. Selection of absorption spectra recorded during the irradiation of **1** in  $\text{CH}_2\text{Cl}_2$  solution with white light. Individual spectra were recorded at regular time intervals covering 450 mins; see Supporting Information for actual times.

In qualitative terms, exposure of the sample dissolved at the micromolar level in deoxygenated  $\text{CH}_2\text{Cl}_2$  to white light leads to slow but progressive bleaching of both BDMA ( $\lambda_{\text{MAX}} = 612$  nm) and BTH ( $\lambda_{\text{MAX}} = 815, 525$  and 440 nm) chromophores (Figure 5). Concomitant with bleaching of the primary chromophores, the spectral changes are consistent with the gradual appearance of new absorption bands at 715 and 560 nm. In turn, these intermediary products degrade under further illumination and the final product mixture possesses absorption bands in the near-UV region ( $\lambda_{\text{MAX}} = 512$  and 450 nm). The sharp absorption band centred at 560 nm is highly reminiscent of the protonated form of BDMA, which was studied earlier as a putative pH probe.<sup>11</sup> Furthermore, the broad absorption profile centred at 715 nm is associated with the BTH unit since the same species arises from direct photolysis of **A1** in deoxygenated  $\text{CH}_2\text{Cl}_2$  (see Supporting Information). Interestingly, both intermediary products fluoresce such that the ability to sensitize a solar cell is not lost during the initial

bleaching process. Furthermore, it was noted that efficient EET occurs from the protonated form of BDMA to the product absorbing at 715 nm. The final, near-UV absorbing species, which does not bleach significantly under our conditions, also retains the ability to sensitize a solar cell. The photochemistry is irreversible, although the overall bleaching efficiency is extremely low (see later). We now consider the three stages of reaction as identified above.

The rates of the initial photo-bleaching step, whereby both BDMA and BTH units degrade, are very similar, if not identical, for each chromophore despite the imbalanced photon intake. This behaviour is not to be expected since the excited-state lifetime of the BDMA donor is extremely short because of intramolecular EET to the proximal BTH component. The excited-state of the latter is relatively long lived and should bleach at a much faster rate than found for the donor unit. Bleaching of BTH is most conveniently followed at 820 nm while that for BDMA can be monitored at 610 nm. For each chromophore, the decrease in absorbance follows a non-linear pattern with respect to illumination time, even at the earliest stages and the rate of bleaching appears to increase with illumination time (Figure 6). This behaviour indicates some kind of autocatalytic process<sup>20</sup> that enhances the rate of photo-bleaching. Leaving the sample overnight in the dark, intended to mimic outdoor conditions, has no effect on the reaction. Further illumination simply continues the bleaching step, for which there are at least 5 isosbestic points across the spectral window (Figures 6 and S5) for the first stage in the overall bleaching chemistry (Scheme 1).

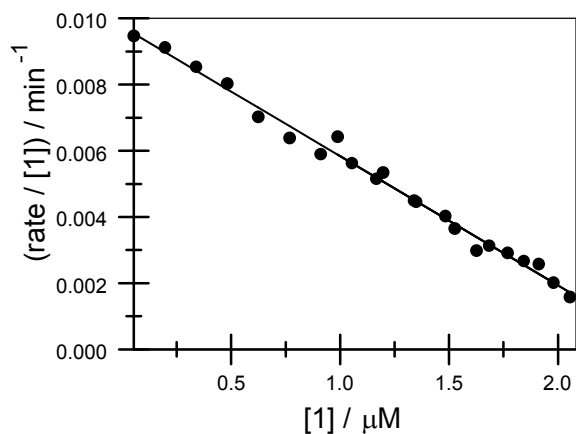


Figure 6. Example of the fitting of experimental data ( $\lambda = 812$  nm) to an autocatalytic process (i.e., Equation 1). The points are experimental measurements and the solid line is a non-linear, least-squares fit to Equation 1.

A reaction is deemed to be autocatalytic<sup>20</sup> when a product-concentration vs time profile is “S-shaped” or when a reaction-rate vs time plot is “bell-shaped” with both an acceleration stage and a decay period. At least two mechanisms must operate, one being responsible for the initial bleaching step and the other making use of a primary product to enhance further bleaching. On the acceptance of *pseudo*-first order conditions being met, this being confirmed by a small concentration

dependence study, the overall reaction rate can be expressed in the form of Equation 1 where  $k_0$  is a rate constant for the initial reaction and  $k_1$  is the corresponding rate constant for the catalysed reaction. Here, the term  $A$  refers to absorbance and the subscripts represent the individual reading (i.e.,  $A_0$  is the first absorbance reading,  $A_1$  is the second reading, etc.). Iterative, least-squares fitting of the photolysis data allows calculation of these two rate constants (Table 2), as determined by global fitting of the early photolysis stage carried out across a wide wavelength region.

$$\frac{A_1 - A_3}{\Delta t_{3,1} [1]_2} = (k_0 - k_1 [1]_0) - k_1 [1]_2 \quad (1)$$

$$k_N = \frac{(A_0 - A_t)}{\Delta t} \cdot \frac{1}{(\epsilon_0 - \epsilon_\infty) [1]_0} \quad (2)$$

**Table 2.** Summary of rate constants associated with the stepwise photo-bleaching of the target array in deoxygenated  $\text{CH}_2\text{Cl}_2$  solution.

Process	Direction	$k / \text{min}^{-1}$ (a)	$\lambda / \text{nm}$ (b)	Statistics (c)
BDMA $\rightarrow$ BDMAH <sup>+</sup>	bleaching	$k_0 = 0.0019$ $k_1 = 0.0039$	605-615	SD = 0.0005; GF = 0.9923
BTH $\rightarrow$ BTH'	bleaching	$k_0 = 0.0017$ $k_1 = 0.0038$	790-830	SD = 0.0002; GF = 0.9954
BTH $\rightarrow$ BTH'	formation	$k_0 = 0.0016$ $k_1 = 0.0038$	710-725	SD = 0.0003; GF = 0.9967
BDMAH <sup>+</sup> $\rightarrow$ BDMAH'	bleaching	$k_2 = 0.0058$	555-565	SD = 0.0854; GF = 0.9960
BTH' $\rightarrow$ BTH''	bleaching	$k_3 = 0.0023$	690-750	SD = 0.0229; GF = 0.9986
BTH' $\rightarrow$ BTH''	formation	$-k_3 =$ 0.0022	425-490	SD = 0.0444; GF = 0.9916

(a) Refer to Scheme 1 for definition of individual rate constants. (b) Wavelength range for global data analysis. (c) SD refers to standard deviation for the fit and GF refers to the goodness-of-fit correlation term.

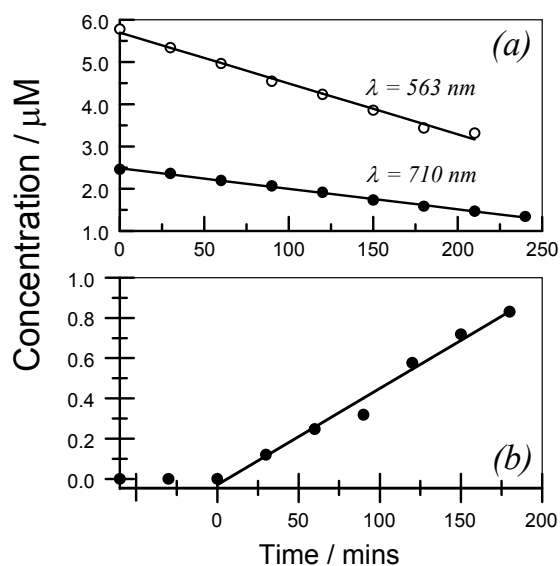
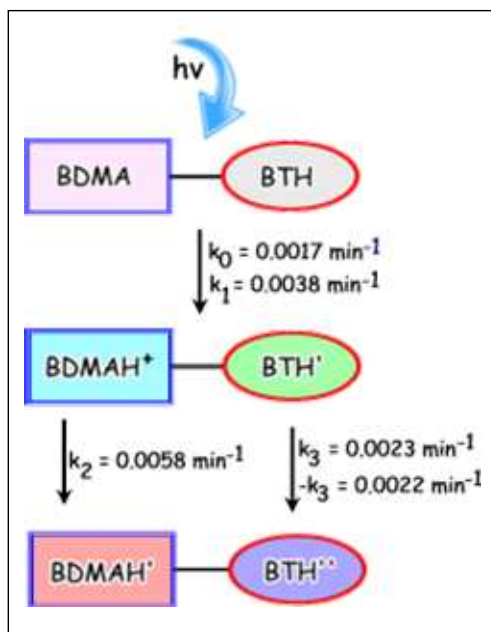


Figure 7. Examples of fitting the experimental data to Equation 2 for (a) degradation of the intermediary products BDMAH<sup>+</sup> ( $\lambda = 563$  nm) and BTH' ( $\lambda = 710$  nm) and (b) formation of the final product, BTH''.

The absorption bands associated with the primary products, as seen at 715 and 560 nm, appear at closely comparable rates, indicating that they share a common reaction pathway, before slowly bleaching under continuous illumination. The rates of secondary photo-bleaching differ for the two absorption bands (Figure 7). Thus, these two species undergo disparate reaction pathways leading to their slow degradation. Notably, disappearance of the protonated form of BDMA (i.e.,  $\text{BDMAH}^+$ ) is essentially linear with photolysis time (Equation 2 where  $\epsilon$  refers to the molar absorption coefficient at that wavelength) but loss of the breakdown product from BTH (monitored at 690-750 nm), which is abbreviated as  $\text{BTH}'$ , involves a short inhibition period before bleaching sets in. For a typical substrate concentration of  $2 \mu\text{M}$ , the rate of bleaching of  $\text{BDMAH}^+$  is about  $12 \text{ nmol dm}^{-3} \text{ min}^{-1}$  (Table 2) while the same analysis shows the decomposition of  $\text{BTH}'$  to occur more slowly with a typical rate of ca.  $5 \text{ nmol dm}^{-3} \text{ min}^{-1}$ .

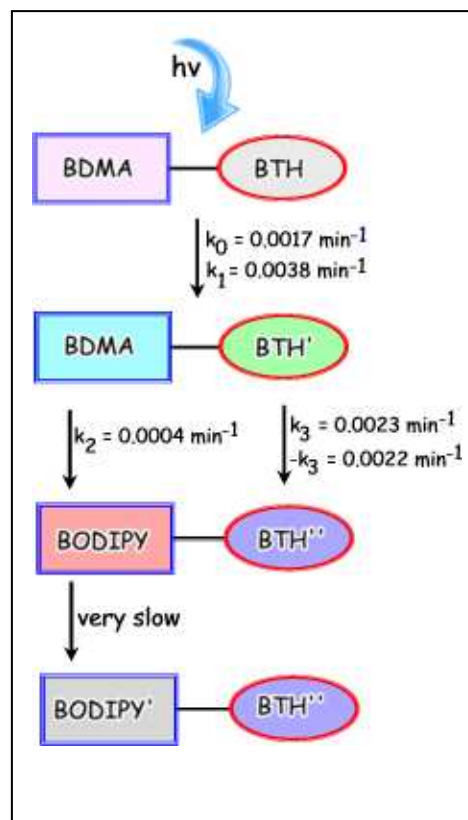
Using the control compound **D1**, after protonation with HCl in  $\text{CH}_2\text{Cl}_2$  solution, it was found that illumination with visible light caused relatively fast bleaching that resulted in a colourless product. In contrast, illumination of  $\text{BTH}'$  leads to a further product that absorbs in the near-UV region. This latter product,  $\text{BTH}''$ , is extremely robust and degrades very slowly under continuous illumination. The rate of formation of  $\text{BTH}''$  agrees remarkably well with the rate of bleaching of  $\text{BTH}'$  (Table 2). The overall reaction scheme leading to degradation of **1** under visible light excitation is summarized concisely by way of Scheme 1.



Scheme 1. Pictorial representation of the processes leading to photo-conversion of the target compound **1** in  $\text{CH}_2\text{Cl}_2$  solution when exposed to simulated sunlight.

Our understanding of the photo-bleaching of the artificial photon harvester **1** in  $\text{CH}_2\text{Cl}_2$  can now be summarised as follows: The compound absorbs over a wide spectral range

covering the entire visible zone and stretching into the far-red region. Integration of the absorption profile indicates that approximately 68% of absorbed photons are directed to the BTH-based acceptor, which shows modest fluorescence centred at around 900 nm. Under visible light illumination, BTH undergoes slow bleaching to form the primary product  $\text{BTH}'$  that shows prominent absorption at around 715 nm. During this bleaching process, at least one proton is released into the system and becomes attached to the BDMA terminal, forming  $\text{BDMAH}^+$ . This protonation step is fast such that bleaching of the BTH and BDMA chromophores occurs at the same rate. As reaction proceeds, one of the resultant products catalyses bleaching of BTH so that the rate increases with time of photolysis. Ultimately, the system reaches the state where  $\text{BTH}'$  and  $\text{BDMAH}^+$  co-exist. Further illumination leads to irreversible bleaching of  $\text{BDMAH}^+$  to form a transparent product and this unit is lost from the system. In contrast, further bleaching of  $\text{BTH}'$  occurs to form the near-UV absorbing species  $\text{BTH}''$ . This latter product does not bleach under our conditions.



Scheme 2. Pictorial representation of the events leading to photo-conversion of **1** in non-protic media when exposed to simulated sunlight.

The origin of the proton that attaches itself to BDMA can be traced to breakdown of the  $\text{CH}_2\text{Cl}_2$  solvent since  $\text{BDMAH}^+$  does not form when the photochemistry is carried out in either tetrahydrofuran (THF) or poly(methylmethacrylate) (PMMA). In fact, it is known that certain aryl amines undergo auto-

catalytic breakdown under photolysis in the presence of carbon tetrachloride.<sup>21</sup> Here, the degradation mechanism might be considered to involve light-induced electron transfer from chromophore to solvent, with subsequent loss of a chloride anion from the  $\text{CCl}_4$  radical anion and addition of a molecule of  $\text{O}_2$  to form a peroxy ( $\text{CCl}_3\text{OO}\cdot$ ) radical. This latter species is well known in radiation chemistry<sup>22</sup> and is capable of causing further oxidative damage.<sup>23</sup> The peroxy radical can also undergo hydrogen abstraction to form a solvent-derived hydroperoxide and this could be the source of the acidic proton.

Photolysis in aprotic THF, illumination causes slow degradation of BTH exactly as described above but there is little loss of BDMA during the early stages of reaction. Instead, this latter chromophore remains intact and able to transfer excitation energy to  $\text{BTH}^\cdot$ . Continued illumination, however, leads to very slow degradation of BDMA to form a primary product absorbing at around 500 nm (Scheme 2). This latter species possesses an absorption spectral profile consistent with a BODIPY derivative lacking the styryl residue.<sup>9</sup> This latter species undergoes extremely slow photo-bleaching, a fact confirmed by separate irradiation of BODIPY in deoxygenated THF solution. Illumination of **1** in PMMA follows the same pattern as seen in THF solution but the course of reaction is too slow to monitor meaningful kinetic parameters, even for thin (i.e., 10  $\mu\text{m}$ ) films.

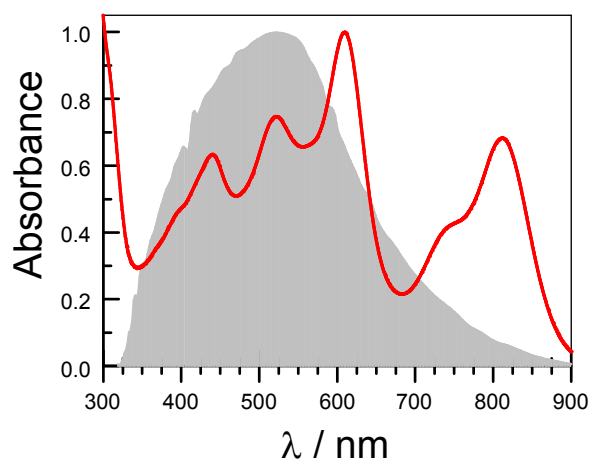


Figure 8. The absorption spectrum recorded for **1** (red curve) in  $\text{CH}_2\text{Cl}_2$  superimposed over that of a thin-film of amorphous silicon deposited onto a flexible plastic substrate.

### Sensitization of amorphous silicon solar cells

Prior to photo-bleaching, **1** emits weakly at 900 nm and, in principle, should be capable of sensitizing a silicon or gallium arsenide solar cell. The fluorescence quantum yield ( $\Phi_F = 0.013$ ) is kept low by partial charge transfer with the terminal amine but could be improved by eliminating this latter component. The product allows for EET from  $\text{BDMAH}^+$  to  $\text{BTH}^\cdot$  and for continued sensitization of the solar cell by way of emission from  $\text{BTH}^\cdot$ . This intermediary product absorbs strongly in the visible region but lacks the ability to harvest

photons in the far-red region. Further degradation to form  $\text{BTH}^\cdot$  is slow and the product is a relatively poor photon collector since it absorbs only at wavelengths below about 600 nm. Nonetheless, it should continue to direct photons to the solar cell. The overall turnover number for one molecule of **1** under continuous illumination with white light exceeds ten million, allowing for all stages of photo-bleaching.

It might be noted that the absorption spectrum of **1** overlaps strongly with that of a thin film of hydrogenated amorphous silicon, a-Si:H, as indicated by way of Figure 8. The organic dye protects the solar cell from exposure to UV-light and strongly amplifies light harvesting in the far-red region where a-Si:H absorbs weakly. Spectral overlap between emission from **1** and absorption by a-Si:H is weak but nonetheless sensitization of the solar cell is possible. This latter point was confirmed by recording action spectra for a thin-film of a-Si:H deposited onto a flexible plastic sheet. The action spectrum (Figure 9), recorded for open-circuit photocurrent measurements, resembles the absorption spectrum recorded for the solar panel (Figure 8). In order to sensitize the solar panel, a rod (diameter 1.2 cm and length 2.5 cm) of PMMA doped with **1** was prepared by slow polymerisation and polished along all surfaces. The solar panel was wrapped along the rod, leaving the ends exposed. A collimated beam of white light was passed through the rod and the resultant photocurrent from the solar panel was recorded (Figure 9). Comparison of the two action spectra clearly shows that the solar cell is sensitized by emission from **1** under these conditions. It should be noted that the set-up was far from being optimal but serves the purpose for proof-of-concept. In particular, the a-Si:H solar panels perform better in terms of current generation when flat so our experimental arrangement is far from ideal.

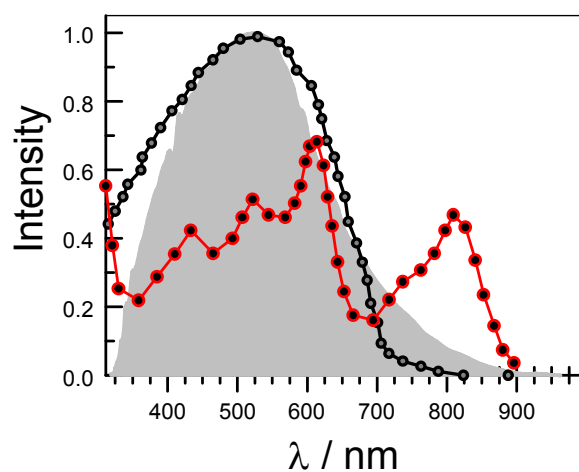


Figure 9. Action spectra recorded for a thin-film a-Si:H flexible solar cell (black points) compared to the absorption spectrum of the panel (grey shadow). The action spectrum recorded for sensitization of a-Si:H by **1** dispersed in PMMA is shown as the red curve.

The most notable feature of the sensitization experiment concerns the enhanced sensitivity towards far-red light (Figure 9). This provides a simple means to protect the solar cell from

undue exposure to blue light, this being a major cause of Staebler-Wronski degradation. Thus, indirect sensitization of the type discussed here could provide an effective means for stabilizing a-Si:H solar cells. It was not possible to confirm this possibility because of the experimental set-up employed, most notably the geometry of the sensitization experiments precludes direct illumination of the solar panel. Instead, we will address this point in a forthcoming article, where we will also explore the underlying mechanism leading to EET from dye to semiconductor.

## Conclusion

The use of artificial light-harvesting arrays to sensitize solar cells is at a very early stage of development<sup>5-7</sup> and it is not yet clear if such devices offer a genuine benefit compared to direct excitation of the semiconductor. Nonetheless, it is an interesting concept that merits proper exploration. One obvious problem relates to the stability of the array under continuous exposure to sunlight<sup>24</sup> and, as such, it is necessary to identify and utilize pigments with exceptional levels of photo-stability. Our approach to this problem has been to introduce a self-protective mechanism whereby photochemical degradation leads to a product that also functions as a useful sensitizer. In this way, the operating timescale is lengthened considerably but there is a certain inevitability that the fraction of solar light harvested by the array decreases at each step. This situation is nicely exemplified by considering the breakdown of **1** in aprotic media. Thus, integration of the absorption spectral profile with respect to a thin-film a-Si:H solar panel indicates about 71% of the spectral distribution is covered by the array. On conversion of BTH to BTH', this value falls to 63% while further reaction to convert BTH' to BTH'' causes a drop to 42%. Conversion of the BDMA unit to BODIPY' is accompanied by a further fall to 31%. The severely damaged array still fulfils its duty as a sensitizer but no longer collects far-red photons. It might be noted that it proved impossible to determine a meaningful quantum yield for photochemical degradation using monochromatic light, even when using a red-emitting laser diode. This is because the rate of decomposition, especially at the onset of the experiment, is too slow to allow accurate monitoring of the course of reaction.

A second lesson learned from this study is the need to select an appropriate medium for the dye; in the case of **1** this translates to the avoidance of protic media. This requires systematic engineering of the system to eliminate problems imposed by the environment. Notably, the presence of molecular oxygen has little effect on the course of reaction and cannot be completely eliminated without encasing the array in a protective cover.<sup>25</sup> It is also important to carefully match the sensitizer with the semiconductor in order to obtain the optimal effect. There are, in fact, clear synergistic effects to be gained by combining a-Si:H with dyes such as **1**. Not only does the dye remove near-UV light, which is harmful to the solar cell, but it also protects the cell from Staebler-Wronski<sup>10</sup> degradation by avoiding direct excitation with blue light.

The approach used here does not permit identification of the breakdown products; using NMR spectroscopy to monitor the fate of a closely related array showed the process to be highly complicated but confirmed that the BODIPY unit absorbing at lowest energy was the first species to photo-bleach. Indeed it is not necessary to identify the products but there is a need to either repair the damaged sites or improve the overall photochemical stability for the long-wavelength absorbing species. The array described here shows a somewhat comparable turnover number to that of chlorophyll in the natural photosynthetic process<sup>26</sup> but we have no provision for either self-repair<sup>27</sup> or photochemical regulation.<sup>28</sup> Such features, which are inherent to the natural process,<sup>26</sup> will be addressed in a forthcoming publication.

## Experimental details

Solvents were purchased from Sigma-Aldrich as spectroscopic grade and were used as received. Absorption spectra were recorded with a Perkin-Elmer Lambda-35 spectrophotometer while emission spectra were recorded with an Hitachi F-4500 spectrofluorimeter. For the far-red emitting samples, specialised facilities were provided by Edinburgh Photonics (a division of Edinburgh Instruments). Fluorescence quantum yields were determined with a fully-corrected, high radiance integrating sphere. Fluorescence lifetimes were determined by time correlated, single-photon counting methods following excitation with an ultra-short laser diode. For steady-state irradiation experiments, the solution was deoxygenated by purging with dry N<sub>2</sub> and sealed into a glass cuvette. The sample was exposed to the white light source (JCC Model IP66, 450W E40) for varying time intervals. The light intensity at the front surface of the cuvette was determined with a PM100 power meter fitted with a Si-photodiode sensor head. Electrochemical measurements were made by cyclic voltammetry using a Pt working electrode, a Ag wire counter electrode and a standard SCE reference electrode. Ferrocene was used as internal standard. The CH<sub>2</sub>Cl<sub>2</sub> solvent was dried and freshly distilled immediately before use while tetra-N-butylammonium perchlorate used as the background electrolyte at a concentration of 0.1 M was recrystallised several times from ethanol and dried under vacuum. A variety of scan rates was used but the quoted data refer to a fixed scan rate of 60 mV per second. All measurements were made under an atmosphere of dry N<sub>2</sub> at room temperature.

Thin films of the dye incorporated into PMMA were prepared by spin coating (Laurell WS-650SZ-6NPP) while thicker films were prepared by simple casting from concentrated solution in CH<sub>2</sub>Cl<sub>2</sub>. The PMMA rod was prepared by *in-situ* polymerization of methyl methacrylate, after removal of the inhibitor by vacuum distillation, using 1,1'-azobis(cyclohexanecarbonitrile) (0.02% w/w) at 10 °C under modest vacuum. The rod was cut to size and polished using very fine 600 grit emery paper.

The amorphous silicon solar panel, presented in the form of a flexible sheet, was provided by Sanyo. Action spectra were

recorded under open circuit conditions using a Sinclair digital current meter and a high-radiance monochromator. The light source was a calibrated 250 W Xe-arc lamp.

Quantum chemical calculations were made with TURBOMOLE<sup>29</sup> running on a multiple processor workstation. Calculations were made at both ground- (DFT/B3LYP/aug-cc-pVTZ) and excited-state (TD-DFT/CAM-B3LYP) levels with the target compound embedded in a solvent continuum using the CPCM model.<sup>30</sup>

### Acknowledgements

We thank the Douglas Bomford Trust, EPSRC-IAA, Newcastle University, CNRS and ECMP-Strasbourg for financial support of this work. We also thank Dr. Anna Gakamsky (Edinburgh Photonics Ltd.) for help with recording the photophysical properties of the far-red emitting dyes.

### Notes and references

<sup>a</sup> Molecular Photonics Laboratory, School of Chemistry, Bedson Building, Newcastle University, Newcastle upon Tyne, NE1 7RU, United Kingdom, Tel: 44 191208 8660; E-mail: anthony.harriman@ncl.ac.uk.

<sup>b</sup> Laboratoire de Chimie Organique et Spectroscopies Avancées, ICPEES-LCOSA, UMR7515, CNRS/ECMP, 25 rue Becquerel, 67087 Strasbourg, Cedex 02, France, E-mail: ziesel@unistra.fr.

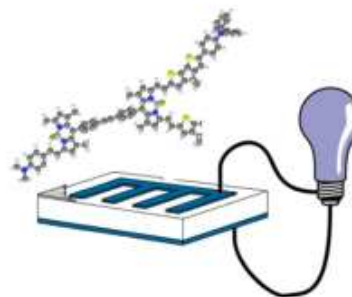
§ Compound **1** was prepared under standard conditions, previously elaborated in the literature,<sup>31</sup> by cross coupling the preformed derivatives **A1** and **D1**<sup>32</sup> in the presence of catalytic amounts of [Pd(PPh<sub>3</sub>)<sub>4</sub>] under mild reaction conditions. Purification by column chromatography on flash silica was straightforward and additional purification was assured by crystallization from suitable solvents. The highly soluble compound **1** was isolated in 71%. The analytically pure deep-brown compound was analyzed by NMR spectroscopy, mass spectrometry and elemental analysis, thereby unambiguously confirming the molecular structure (see Supporting Information). In particular, the mass spectral analysis revealed a molecular peak at 2000.1 amu with successive fragments assigned to the release of fluorine atoms [at 1981.1 (35%), 1962.2 (15%)] amu.

Electronic Supplementary Information (ESI) available: [spectroscopic characterization of new compounds, energy-minimized structures for **A1**, **D1** and **1**, details for estimation of  $\Delta G_{CT}$ , version of Figure 5 showing reaction times, spectra showing photo-conversion of **A1**]. See DOI: 10.1039/b000000x/

- 1 D. Beljonne, C. Curutchet, G. D. Scholes and R. J. Silbey, Beyond Forster resonance energy transfer in biological and nanoscale systems, *J. Phys. Chem. B*, 2009, **113**, 6583-6599.
- 2 J. S. Wu, W. M. Liu, J. C. Ge, H. Y. Zhang and P. F. Wang, New sensing mechanisms for design of fluorescent chemosensors emerging in recent years, *Chem. Soc. Rev.*, 2011, **40**, 3483-3495.
- 3 C. H. Fan, K. W. Plaxco and A. J. Heeger, Biosensors based on binding-modulated donor-acceptor distances, *Trends Biotechnol.*, 2005, **23**, 186-192.
- 4 V. Balzani, Photochemical molecular devices, *Photochem. Photobiol. Sci.*, 2003, **2**, 459-476.

- 5 R. Ziessel and A. Harriman, Artificial light-harvesting antennae: Electronic energy transfer by way of molecular funnels, *Chem. Commun.*, 2011, **47**, 611-631.
- 6 A. C. Benniston, A. Harriman and S. Yang, Providing power for miniaturized medical implants: Triplet sensitization of semiconductor surfaces, *Phil. Trans. Royal Soc. A*, 2013, **371**, art. number 20120334.
- 7 R. Ziessel, G. Ulrich, A. Haeefele and A. Harriman, An artificial light-harvesting array constructed from multiple Bodipy dyes, *J. Am. Chem. Soc.*, 2013, **135**, 11330-11344.
- 8 B. A. Gregg, Excitonic solar cells, *J. Phys. Chem. B*, 2003, **107**, 4688-4698.
- 9 G. Ulrich, R. Ziessel and A. Harriman, The chemistry of fluorescent Bodipy dyes: Versatility unsurpassed, *Angew. Chem., Int. Ed.*, 2008, **47**, 1184-1201.
- 10 A. Klaver and R. A. van Swaaij, Modelling of light-induced degradation of amorphous silicon solar cells, *Solar Energy Mater. Solar Cells*, 2008, **92**, 50-60.
- 11 (a) N. Boens, V. Leen and W. Dehaen, Fluorescent indicators based on BODIPY, *Chem. Soc. Rev.*, 2012, **41**, 130-1172. (b) A. Nano, P. Retailleau, J. P. Hagon, A. Harriman and R. Ziessel, A hybrid bis(amino-styryl) substituted Bodipy dye and its conjugate diacid: Synthesis, structure, spectroscopy and quantum chemical calculations, *Phys. Chem. Chem. Phys.*, 2014, **16**, 10187-10198.
- 12 J. R. Bolton and M. D. Archer, Calculation of natural radiative lifetimes from absorption and fluorescence properties of semiconductors and molecules, *J. Phys. Chem.*, 1991, **95**, 8453-8461.
- 13 T. Bura, N. Leclerc, S. Fall, P. Leveque, T. Heiser, P. Retailleau, S. Rihn, A. Mirloup and R. Ziessel, High-performance solution-processed solar cells and ambipolar behavior in organic field effect transistors with thienyl-BODIPY scaffolding, *J. Am. Chem. Soc.*, 2012, **134**, 17404-17407.
- 14 A. Harriman, G. Izzet and R. Ziessel, Rapid energy transfer in cascade-type Bodipy dyes, *J. Am. Chem. Soc.*, 2006, **128**, 10868-10875.
- 15 R. E. Dale, J. Eisinger and W. E. Blumberg, Orientational freedom of molecular probes - orientation factor in intramolecular energy transfer, *Biophys. J.*, 1979, **26**, 161-193.
- 16 P. G. Wu and L. Brand, Resonance energy transfer - methods and applications, *Anal. Biochem.*, 1994, **218**, 1-13.
- 17 V. Czikkely, H. D. Forsterling and H. Kuhn, Extended dipole model for aggregates of dye molecules, *Chem. Phys. Lett.*, 1970, **6**, 207-210.
- 18 R. Ziessel, P. Retailleau, K. J. Elliott and A. Harriman, Boron dipyrin dyes exhibiting push-pull-push electronic signatures, *Chem. Eur. J.*, 2009, **15**, 10369-10374.
- 19 M. R. Wasielewski, Photoinduced electron-transfer in supramolecular systems for artificial photosynthesis, *Chem. Rev.*, 1992, **92**, 435-461.
- 20 F. Mata-Perez and J. F. Perez-Benito, The kinetic rate law for autocatalytic reactions, *J. Chem. Ed.*, 1987, **64**, 925-927.
- 21 a) O. M. Usov, M. I. Bardamova and I. L. Kotlyarevskii, Photochemistry of acetylenic derivatives of aromatic amines. 1. Photolysis products of paraethynyl-N,N-dimethylaniline in carbon tetrachloride. *Bull. Acad. Sci. USSR Div. Chem. Sci.*, 1986, **35**,

- 1055-1057. b) M. I. Bardamova and O. M. Usov, Photochemistry of acetylenic derivatives of aromatic amines. 2. Photolysis of para-ethynyl-N,N-dibenzylaniline and para-butadiynyl-N,N-dibenzylaniline in the presence of carbon tetrachloride and oxygen. *Bull. Acad. Sci. USSR Div. Chem. Sci.*, 1986, **35**, 1055-1057.
- 22 Z. B. Alfassi, A. Harriman, S. Mosseri and P. Neta, Rates and mechanisms of oxidation of ZnTPP by  $\text{CCl}_3\text{O}_2$  radicals in various solvents. *Int. J. Chem. Kinet.*, 1986, **18**, 1315-1321.
- 23 a) H. D. Burrows, T. J. Kemp and D. Greatore, Solute radical cation yields in pulse radiolysis of solutions of aromatic amines in chlorinated hydrocarbons. *J. Phys. Chem.* 1972, **76**, 20-27. b) H. D. Burrows, T. J. Kemp and M. J. Welbourn, Intermediates in the pulse radiolysis of solutions of phenothiazine and its derivatives - Reactions of cycloalkylperoxy radicals with phenothiazines. *J. Chem. Soc., Perkin Trans. 2*, 1973, 969-974.
- 24 S. Wennmalm and R. Rigler, On death numbers and survival times of single dye molecules, *J. Phys. Chem. B*, 1999, **103**, 2516-2519.
- 25 H. S. Weerasinghe, S. E. Watkins, N. Duffy, D. J. Jones and A. D. Scully, Influence of moisture out-gassing from encapsulant materials on the lifetime of organic solar cells. *Solar Energy Mater. Solar Cells*, 2015, **132**, 485-491.
- 26 a) A. A. Pascal, Z. F. Liu, K. Broess, B. van Oort, H. van Amerongen, C. Wang, P. Horton, B. Robert, W. R. Chang and A. Ruban, Molecular basis of photoprotection and control of photosynthetic light-harvesting, *Nature*, 2005, **436**, 134-137. (b) G. Peers, T. B. Truong, E. Ostendorf, A. Busch, D. Elrad, A. R. Grossman, M. Hippler and K. K. Niyogi, An ancient light-harvesting protein is critical for the regulation of algal photosynthesis, *Nature*, 2009, **462**, 518-522.
- 27 H. R. Bolharnordenkamp, M. Hofer and E. G. Lechner, Analysis of light-induced reduction of the photochemical capacity in field-grown plants – evidence for photoinhibition, *Photosynth. Res.*, 1991, **27**, 31-39.
- 28 P. Horton, A. V. Ruban and M. Wentworth, Allosteric regulation of the light-harvesting system of photosystem II, *Phil. Trans. Royal Soc. B*, 2000, **355**, 1361-1370.
- 29 R. Ahlrichs, M. Bär, M. Häser, H. Horn, and C. Kölmel, "Electronic structure calculations on workstation computers: The program system Turbomole", *Chem. Phys. Lett.*, 1989, **162**, 165-169.
30. (a) V. Barone and M. Cossi, *J. Phys. Chem. A*, 1998, **102**, 1995-2001. (b) H. Li and J. H. Jensen, *J. Comput. Chem.*, 2004, **25**, 1449-1456.
- 31 R. Ziessel, S. Rihn and A. Harriman, Quasi-one-dimensional electronic systems formed from boron dipyrromethene (BODIPY) dyes, *Chem. Eur. J.*, 2010, **16**, 11942-11953.
- 32 A. Sutter and R. Ziessel, A versatile synthesis of long-wavelength-excitabile BODIPY dyes from readily modifiable cyclopenta[2,1-b:3,4-b']dithiophenes, *SynLett*, 2014, **25**, 1466-1472.



The target light-harvesting antennae can be used to sensitize a solar cell in order to improve its performance.